December 16, 2003

Journal of Biomedical Optics

Design, testing and clinical studies of a hand-held polarized light camera

Jessica C. Ramella-Roman, Ken Lee, Scott A. Prahl, Steven L. Jacques

1 Oregon Medical Laser Center, Providence St. Vincent Medical Center, Portland, OR

2 Oregon Health & Science University, Portland, OR

Correspondence:

Steven L. Jacques
Oregon Medical Laser Center
9205 SW Barnes Rd
Portland, OR 97225
503-216-4092 phone
503-216-2422 fax
sjacques@ece.ogi.edu

Keywords:

Polarized light, imaging, tissue optical properties, light transport

ABSTRACT

Polarized light imaging has been used to detect the borders of skin cancer and facilitate assessment of cancer boundaries. A design for an inexpensive hand-held polarized camera is presented and clinical images acquired with this prototype are shown. The camera was built with two USB color video cameras, a polarizing beam-splitter cube and a 4x objective lens. Illumination was provided by 3 white LEDs and a sheet polarizer. Horizontal and vertical linearly polarized reflected images were processed at 7 frames per second and a resulting polarized image was displayed on screen. We compared the performances of cheap USB camera and a 16-bit electronically cooled camera. Dark noise and image repeatability were compared. In both cases the 16-bit camera outperformed the USB cameras. Despite these limitations the results obtained with thisUSB prototype were very satisfactory. Examples of polarized images of lesions taken prior to surgery are presented.

INTRODUCTION

Polarized light imaging has been shown [1,2] to give relevant information on the borders of skin cancers that are not visible to the naked eye. Skin cancers typically originate in the superficial regions of the skin (epidermal basement membrane) where polarized light imaging is most effective. Quick assessment of skin cancer margins before Mohs surgery could guide the doctor during excision and reduce the surgery time and patient discomfort. A number of polarized light camera systems have been used in the clinic [3, 4, 5, 6] but routine use has been limited by such factors as size, weight, cost, and poor user interface. Commercially available system such as Dermlite® photo and

Dermlite® platinum (3 Gen, LLC, Dana Point, CA) based on cross-polarization imaging yielded good results [7]. These system are useful for eliminating glare and shadows from the field of view but do not provide information on the backscattered degree of polarization and superficial light scattering. More complex systems based on confocal microscopy [8, 9, 10] allow high resolution, imaging the dermis to 500 μm but with much higher equipment cost and limited portability. In this paper, a simple design is presented for a fully automatic polarized light camera system that can be held with one hand.

The camera system is composed of two USB video cameras, one polarizing beam-splitter cube and a microscope objective lens. A USB-wired mouse button on the camera allows the operator to request image acquisition. The total cost of the prototype system is approximately 350 dollars not including the computer. The hand-held device is controlled and powered through USB connections to a laptop computer. The entire system fits in a computer bag.

MATERIALS AND METHODS

The main components of the hand-held polarization system are visible in Figure 1. Two USB digital cameras (Quickcam Pro3000; Logitech Inc., Fremont, CA, USA 24-bit, 8-bit per color channel) were disassembled and the CCD chips with support electronics were mounted on a Delrin mount that encased a broadband polarizing beam splitter cube (Melles Griot, Carlsbad, CA, USA). The beam-splitter cube had 0.01 nominal polarization extinction and was used to separate the two states of linear polarization, i.e., parallel and perpendicular to the orientation of the polarized source.

Each camera had color 1/4" CCDs capable of acquiring 30 frames/second with an image size of 640x480 pixels. An interchangeable objective lens allowed different magnifications. An objective lens (PL 4/0.1) mounted at a distance of 5 cm from the front

of the beam-splitter cube was the most commonly used imaging assembly. This lens sets the camera's field of view at 1.5x1.2 cm.

The CCDs and beam-splitter cube were encased in an ergonomic plastic sphere as shown in Figure 2. The spherical case protected the components and supported the light source and the focal distance assembly.

The polarized light source was constructed using three ultrabright white LEDs mounted on an acrylic support. The LEDs were battery powered by three AA batteries stored in a compartment in the bottom of the sphere. LED light was linearly polarized parallel to the source-sample-detector plane by a sheet polarizer of extinction 0.0001 (Hinds Inc., Portland, Oregon). The light source assembly was oriented at approximately 30 degree to the objective lens axis to avoid glare.

A fixed distance between the imaging plane and the cameras was maintained using an adjustable acrylic support with a mount for a glass microscope cover slip that constituted an optical flat. During operation, the glass cover slip wasplaced in contact with the skin. A drop of water was used to minimize tissue-air-glass reflections.

The USB cameras were connected to a 667 Mhz PowerBook laptop (Apple Computer Inc., Cupertino, CA, Model # A1001). The controlling software was written in C starting from the QuickTime Software Development Kit (SDK) [11,12]. QuickTime is a system-level code package available on most computers that support multimedia tasks. Images were acquired sequentially from two devices, Camera 1 and Camera 2. Camera parameters such as gain, shutter aperture and window orientation were modifiable through a user menu. During experiments, the gain was fixed and the shutter aperture was kept equal for both cameras. After streaming from the two cameras, every frame was decompressed. The separate frames were aligned (pixel shift respectively x = 10 pixel y=

13 pixels) in the software. A polarized image Pol was calculated at each pixel in the red, green and blue channels:

$$Pol = \frac{parallel - perpendicular}{parallel + perpendicular} \qquad \text{(eq. 1)}$$

where parallel is the image from Camera 1 and perpendicular is the image from Camera 2 (Fig. 1). A composite color image was generated from the three Pol images and displayed on screen. Alternatively, either the red, green, or blue Pol image could be displayed on the screen by pressing the R, G, or B key on the computer. A second window on the screen displayed the original color parallel image to facilitate camera positioning.

The maximum frame rate in order to display the polarized light image in a full size window (400x400 pixels) was 7 frames/sec. The frame rate could be improved by decreasing the image size. When the window was 250x250 pixels the frame rate increased to 15 frames/sec. The software allowed the user to average up to 20 Pol images before displaying the results on screen. Images were on 256 gray levels, typical polarized images intensities were from 20 to 80 counts.

The operator could save a desired image by pressing the USB mouse button on the camera. Images were saved in the Apple PICT image format.

Acrylamide gels were used as standards. Gels were prepared with Intralipid (Liposin II, Abbott Laboratories, North Chicago, IL) and India ink (No. 4415, Higgs, Lewisburg, TN) to illustrate the variability of polarization and reflectance in an amorphous sample. The concentration of the Intralipid was 3.5% (gram lipid/ml solution times 100%). The gels were prepared with acrylamide solution (40% concentration) and water to a final volume of 100ml (4 cm height and 5 cm diameter). The absorption coefficient of the gel was μ_a= 1 cm^{-1} and the scattering coefficient μ_s = 3 cm^{-1}.

System Calibration

Experiments were conducted to test the performance of the cameras and polarizing optics.

Camera dark noise: This test was performed with the camera software shutter off. The test was performed in the dark and dark images were captured at increasing time intervals. Camera streaming was interrupted only during an image save. The camera was run for two hours although typical clinical use of the camera is much brief. The 12 captured images were processed using Matlab software. The mean and standard deviation was calculated for 400x400x12 = 192,000 image pixels, for the three (red, green and blue) images. The blue channel dark noise was the highest at 31 counts (standard deviation = 3 counts) where full-scale response ranged from 0 to 255 counts. The red and green channels dark noise was 15 counts (standard deviation = 3 counts). For all channels, dark noise did not vary over time allowing us to subtract it from the acquired images programmatically. For comparison the same dark noise experiments were performed for a 16-bit digital camera electronically cooled camera (Roper Scientific, Tucson, AZ). The dark noise was approximately 500 counts where the full-scale response ranged from 1-65453.

Camera repeatability: This test was performed to establish the pixel-to-pixel variation during multiple acquisitions. The target was a checkerboard consisting of dark black squares and bright white squares. A group of 20 images of the checkerboard was captured over a 10 minutes period. The variability from image to image was analyzed using Matlab. Different pixel locations were chosen on the images. For every pixel location in both black and white squares the standard deviation of the 20 images was calculated and was less than 3 counts, showing the degree of image-to-image repeatability. A similar test performed

with the 16-bit digital camera gave a pixel-pixel variation of 20 counts. Once again the scientific camera outperform the cheap USB cameras. Currently small scientific 8-bit digital cameras are being considered to replace the USB camera in the design of a better prototype.

Polarization optics The performances of the polarizing beam-splitter and source polarizer were tested in transmission mode. The polarized white light source was positioned in front of the hand-held system behind a linear polarization filter (Ealing Inc, Rocklin, CA) with its polarization axis aligned parallel to the beam splitter horizontal axis. The source polarizer was rotated in 10 degree intervals. At each angle two images were collected: one with Camera 1 (Parallel) and one with Camera 2 (Perpendicular). The transmitted light beam filled most of the cameras' field of view. The pixel intensity counts of the central 100 x 100 pixels were selected to eliminate any beam shape artifact. Dark noise was subtracted from every image.

$$Pol = \frac{(camera1 - Background) - (camera2 - Background)}{(camera1 - Background) + (camera1 - Background)} =$$

$$= \frac{camera1 - camera2}{camera1 + camera1 - 2Background}$$

Results are shown in Figure 3. The mean and standard deviation of all three camera channels, red diamonds, green crosses and blue circles are plotted versus the source polarization angle. The data was normalized by the incident 0° degree value for Camera 1 and incident 90° degree value for Camera 2. The experimental data was modeled with Malus' law: $I = \cos^2\theta$, where θ is the source polarization angle. The model appear as lines in Figure 3.

Back-scatter from microsphere solutions: A solution of 2-μm-diameter microspheres (Fullam Inc. Latham, New York, NY) was diluted until the scattering coefficient was equal to 29 cm^{-1}. The concentration was confirmed with a submerged optical fiber measurements of the lateral diffusion of light from a point source as a function of distance from the source [13]. A rectangular cuvette with an optical path-length of 1.2 cm was filled with the diluted solution. A red He-Ne laser (Melles Griot, Carlsbad, CA, USA) was used for the experiment. The laser beam had a nominal wavelength of 632.8 nm, the beam size was 2 mm and was polarized parallel to the optical bench and the horizontal axis of the beamsplitter. The beam illuminated the cuvette at 10° relative to the cuvette normal. The polarized system was located normal to the cuvette. The image of the polarized image of light reflected from the microsphere solution is shown on the left-hand side of Figure 4. The right side shows the results of a Monte Carlo simulation for this experiment. The Monte Carlo image was obtained with a code [14] that keeps track of the polarization of the photon after every scattering event. For the Monte Carlo program, a slab-geometry was used that did not consider the air-glass interface, which might explain the discrepancies between model and experiment. The structure of the Monte Carlo program was similar to the one written by Kattawar *et al.* described in reference [15]. 10^7 photons were used for the simulation. In both images a Maltese cross scattering pattern was clearly observed and is typical of this kind of experiment.

RESULTS

Clinical studies were conducted at the Department of Dermatology, Oregon Health & Science University. Consent to take part in this study was obtained from all patients. A study protocol was defined and approved by the Hospital IRB Committee. Detailed written and oral information on the protocol was given to the patients prior to

enrollment. The measurements extended the dermatoscopic procedure by an average of 10 minutes.

Images of different skin lesions were captured minutes before Mohs surgery. All images reported were in 256 gray levels. Figure 5a and 5b are images of a melanoma *in situ*. The image in figure 5a was obtained with the parallel polarized camera and normalized by the average pixel value of an image of an epoxy standard and multiplied by 0.65 to yield reflectance. The epoxy standard had 65% calibrated reflectance across the visible wavelength spectrum corresponding to 180 counts.

Melanoma is comprised of abnormal proliferation of the melanocytes, the melanin pigment producing cells in the skin. Melanosomes are organelles that contain melanin.

In the polarized regions with melanin pigmentation are whiter than the amelanotic regions. The whiter regions correspond to the more darkly pigmented globules in the normal image and likely correlate with cluster/nests of melanocytes. In the normal image only gray shades are visible.

To illustrate the potential of the camera system two regions of interest were selected in both figure 5a and 5b. As indicated by the squared areas demarcated by white contour lines corresponding to non-pigmented tissue (N) and melanotic (M). The pixel values for Pol and reflectance within the two regions of interest are cross-plotted in Figure 6. The values of reflectance for a visually normal area (N) are in the 60% range while the values for the melanotic areas (M) are around 45%.

The variation of Pol and R for the amorphous gel sample indicate the noise level in the camera system. The Normal skin site presented a slightly greater range of Pol and R values indicating the natural variation for that skin site. The Melanin skin site presented the largest variation in Pol and R values, with Pol variation greater than the R

variation. The R values of the Melanin site were lower due to incresed melanin content. The increase in Pol for the Melanin site is presumably due to the backscatter of polarized light from the melanosomes.

The Melanin and normal tissues are distinguished on the basis of both Pol and R, with R providing better contrast than Pol. To simply identify melanin in a skin site, R is better than Pol. However, Pol images present more texture in the images. Texture is represented in figure 6 by a greater range of variation in the Pol values relative to the R values. The texture of the melanotic lesion is greater than the texture of the normal skin site. The Pol image offers a better presentation of the variegation of the melanotic lesion.

Figure 7 shows images of a nevus from a forearm. The polarized image is shown on the left and the unpolarized image on the right. In the polarized image the nevus appears white and the background tissue appears dark gray. The structure of the nevus appears hilly and non-uniform. These structures are not visible in the unpolarized image.

Figure 8 shows a squamous cell carcinoma before excision. On the left is the polarized image, and on the right is the normal image. In the normal image are visible specular(white spots) artifacts due to air bubbles between the skin and the opticalflat.

In Figure 9 another melanoma image is shown. In the polarized image, branches of spreading melanoma are visible, while in the normal image the melanoma is visible as darker areas.

DISCUSSION

A hand-held device has been described that can quickly collect polarized light images. Most of the device's parts are available at any computer store. The device costs

approximately 350 dollars. Although its performance is not as good as a cooled 16-bit camera [3], the resulting images contain enough contrast for a preliminary diagnosis of skin cancer margins. Since USB video performance is continuously improving, the gap between bench-top prototypes and hand-held devices of this kind is bound to decrease rapidly.

ACKNOWLEDGMENT

The authors would like to acknowledge Dr. Paulo R. Bargo his for help in the design of the backscattering from microsphere test.

This research was supported by the National Institute of Health grants ROI-CA80985 and R24-EB000224 (S.L.Jacques)

5. REFERENCES

1. R.R. Anderson "Polarized light examination and photography of the skin." Arch Dermatol 127:1000–1005, (1991)

2. S.L. Jacques, J.Roman, K. Lee "Imaging Superficial Tissues With Polarized Light" Lasers Surg. Med. 26:119–129, (2000)

3. S. L. Jacques, J.C. Ramella-Roman, and K. Lee, "Imaging skin pathology with polarized light," Journal of Biomedical Optics. Vol. 7, No. 3, 329-340 (2002)

4. M.H. Smith, P. Burke, A. Lompado, E. Tanner, L.W. Hillman "Mueller matrix imaging polarimetry in dermatology" Proceedings of SPIE Vol. 3911, (2000).

5. J.A. Muccini, N. Kollias, S.B. Phillips, R.R. Anderson, A.J. Sober, M.J. Stiller, L.A. Drake. "Polarized light photography in the evaluation of photoaging," J Am Acad Dermatol; 33:765-769.(1995)

6. S. Gonzalez, M. Rajadhyaksha, R.R. Anderson, "Non-invasive (real-time) imaging of histologic margin of a proliferative skin lesion in vivo," J Invest Derm;111(3):538-539. (1998)

7. G. Argenziano, G. Fabbrocini, P. Carli, V. De Giorgi, E. Sammarco, M. Delfino "Epiluminescence Microscopy for the Diagnosis of Doubtful Melanocytic Skin Lesions" Arch. Dermatol.; 134:1563-1570 (1998)

8. R. Langley, M. Rajadhyaksha, P. Dwyer, A. Sober, T. Flotte, R.R. Anderson. "Confocal Scanning Laser Microscopy of Benign and Malignant Melanocytic Skin Lesions In Vivo". Journal of the American Academy of Dermatology; Volume 45, 365-376 (2001)

9. S. González, Sackstein, M. Rajadhyaksha, R.R. Anderson "Real-time evidence of in vivo leukocyte trafficking in human skin by reflectance confocal microscopy" Journal of Investigative Dermatology. Letter to the Editor, Volume 117, 384-386, (2001)

10. K Busam, K Hester, C. Charles, D. Sachs, C. Antonescu, S. González, A. Halpern, "Detection of Clinically Amelanotic Malignant Melanoma and Assessment of Its Margins by In Vivo Confocal Scanning Laser Microscopy (CSLM)". Arch Dermatol.; 137:923-929 (2001)

11. developer.apple.com

12. G. Towner, "Discovering Quicktime", Morgan Kauffman, San Francisco (1999)

13. P. R. Bargo, S. A. Prahl, and S. L. Jacques, "Optical properties effects upon the collection efficiency of optical fibers in different probe configurations," IEEE-Journal of Select Topics in Quantum Electronics, Vol. 9, No. 2, (2003).

14. J. C. Ramella-Roman, S. A. Prahl, S. L. Jacques "Three polarized light Monte Carlo programs, a performance comparison" (In preparation)

15. G. W. Kattawar and G.N. Plass "Radiance and Polarization of Multiple Scattered Light from Haze and Clouds" Applied Optics Vol 7, No. 8 (1968)

FIGURE LEGENDS

Figure 1: The main components of the hand-held polarization system. The top figure show the main components of the system: polarizing beam-splitter cube, two CCD cameras and an objective lens. The bottom figure is a top view of the set-up showing the CCD cameras attached to a Delrin support enclosing the beam-splitter cube.

Figure 2: The clinical hand-held polarization system, spherical casing protects the main components and makes the prototype easy to hold with one hand.

Figure 3 Performance test for polarized optics. The x-axis denotes the angle of orientation of the linear polarization of the light source (0Ỿ denotes parallel to horizontal axis of beamsplitter). The y-axis denotes the detected intensity for the red, green and blue channels of the two cameras (at x-axis equal to 0Ỿ, the parallel CCD 1 camera sees maximum light and the perpendicular CCD 2 camera sees minimum light).

Figure 4 Monte Carlo model and experimental results of a 633-nm wavelength laser beam scattering from a solution of 2- m microspheres in water. On the left is the plot of the experimental polarized image, and on the right is the corresponding plot of the Monte Carlo model.

Figure 5a: Normal image of melanoma in situ. Each pixel of the reflectance image was normalized by the average value of a 65% reflectance standard and multiplied by 0.65.

White squares denote regions of interest, nonpigmented/amelanotic (N) and melanotic (M), from which data for Fig. 6 is collected.

Figure 5b: Polarized image of melanoma. White squares denote regions of interest, nonpigmented/amelanotic (N) and melanoma (M), from which data for Fig. 7 is collected. In this image the grayscale levels are 256.

Figure 6: Probability density functions, p(Pol, R), showing the distribution of pixel values versus Pol and R for the visible melanin skin site (M), the non-pigmented normal skin site (N), and the standard gel (G). The p(Pol,R), in units of $[R^{-1}\ Pol^{-1}]$, is normalized such that the integral of p(Pol,R) for each sample is unity. The greater variation in Pol relative to R for the melanotic site (M) indicates how Pol images present more texture in an image of a variegated melanotic skin lesion.

Figure 7: Image of a nevus. The apparent textural structure of the nevus is visible in the polarized image on the left, the grayscale levels of the polarized image were 256. The normal image on the right does not show this structure.

Figure 8: Polarized (left) and normal (right) image of a squamous cell carcinoma on a patient's upper lip. The grayscale levels of the polarized image were 256.

Figure 9: Image of a melanoma on a patient's nose. The melanoma appears dark in the normal image (right) and white in the polarized image. The arrows show branches of the spreading melanoma. This entire area was excised during surgery. The grayscale levels of the polarized image were 256.

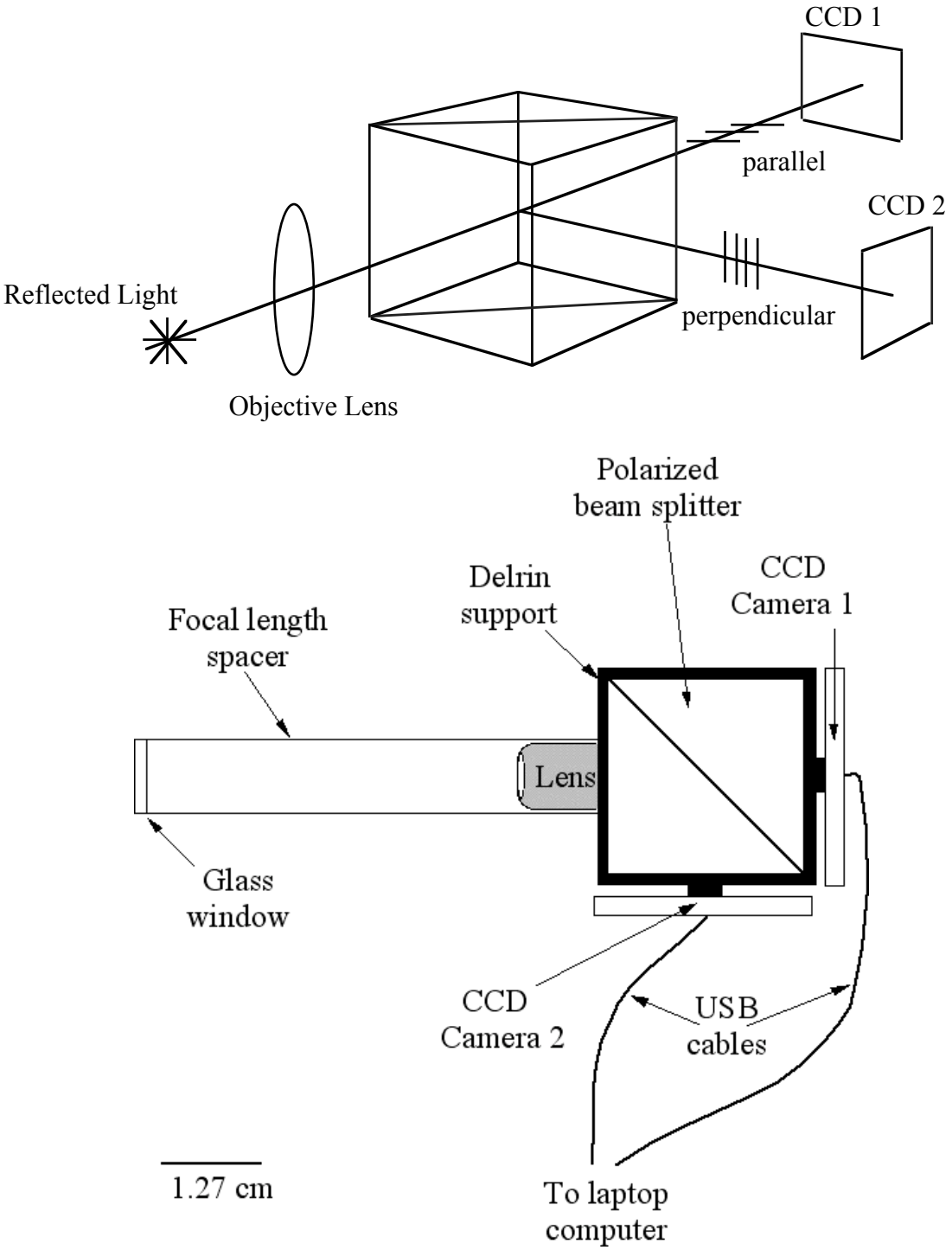

Figure 1: The main components of the hand-held polarization system. The top figure show the main components of the system: polarizing beam-splitter cube, two CCD cameras and an objective lens. The bottom figure is a top view of the set-up showing the CCD cameras attached to a Delrin support enclosing the beam-splitter cube.

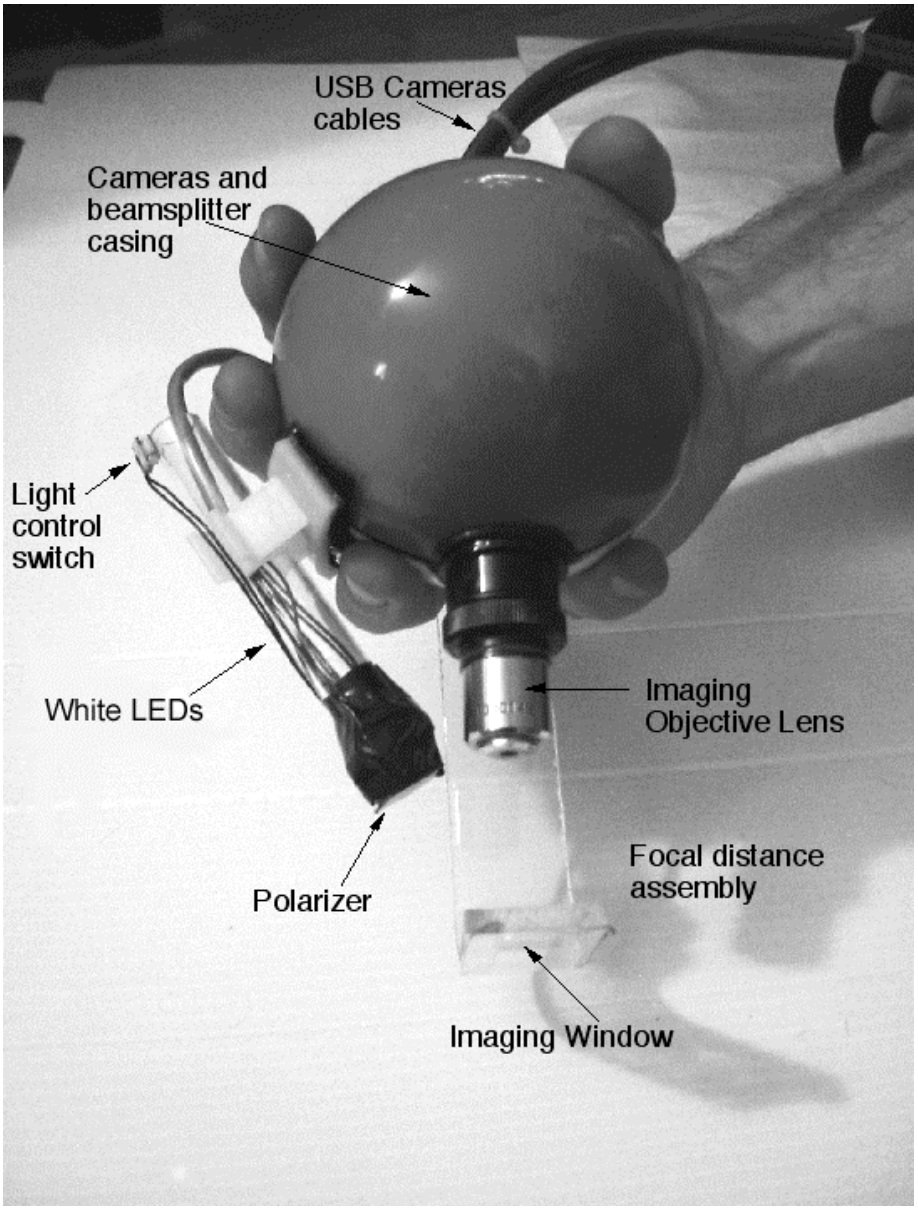

Figure 2: The clinical hand-held polarization system. Spherical casing protects the main components and makes the prototype easy to hold with one hand.

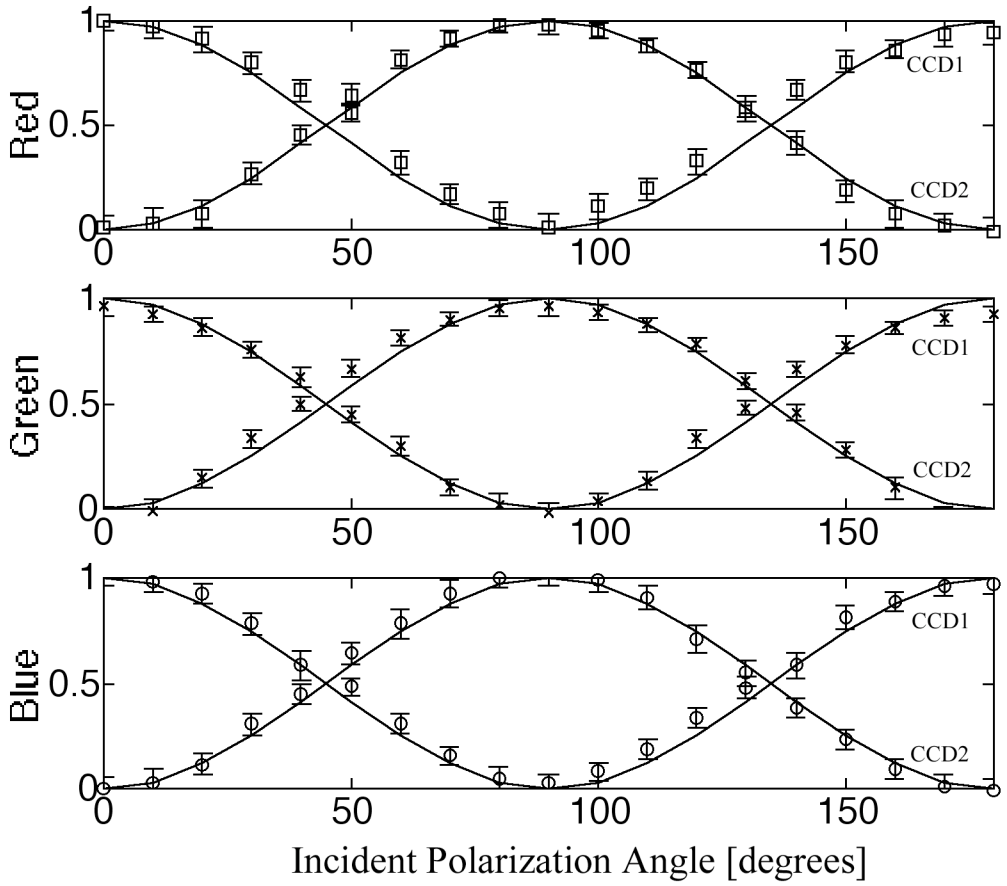

Figure 3 Performance test for polarized optics. The x-axis denotes the angle of orientation of the linear polarization of the light source (0Ύ denotes parallel to horizontal axis of beamsplitter). The y-axis denotes the detected intensity for the red, green and blue channels of the two cameras (at x-axis equal to 0Ύ, the parallel CCD 1 camera sees maximum light and the perpendicular CCD 2 camera sees minimum light).

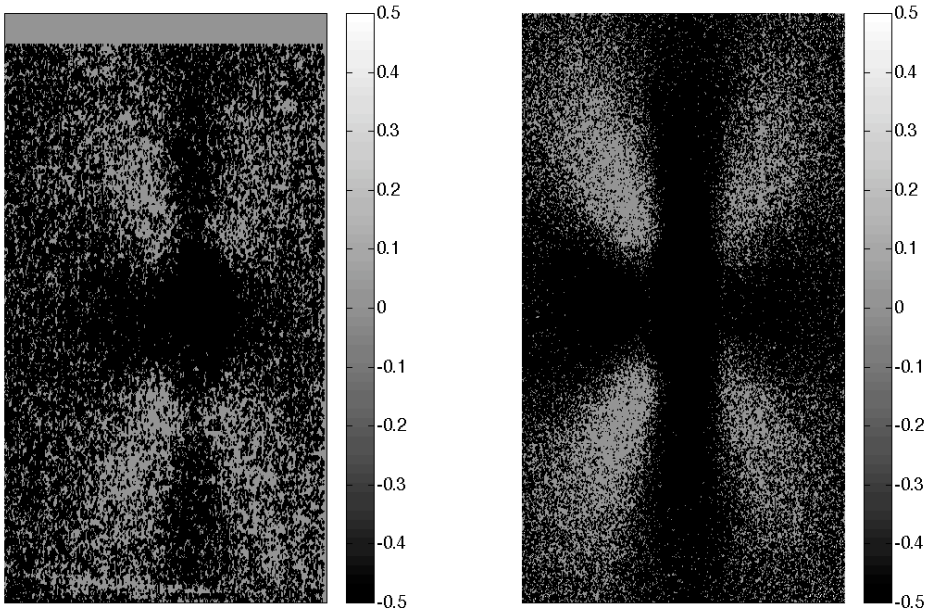

Figure 4 Monte Carlo model and experimental results of a 633-nm wavelength laser beam scattering from a solution of 2- m microspheres in water. On the left is the plot of the experimental polarized image, and on the right is the corresponding plot of the Monte Carlo model.

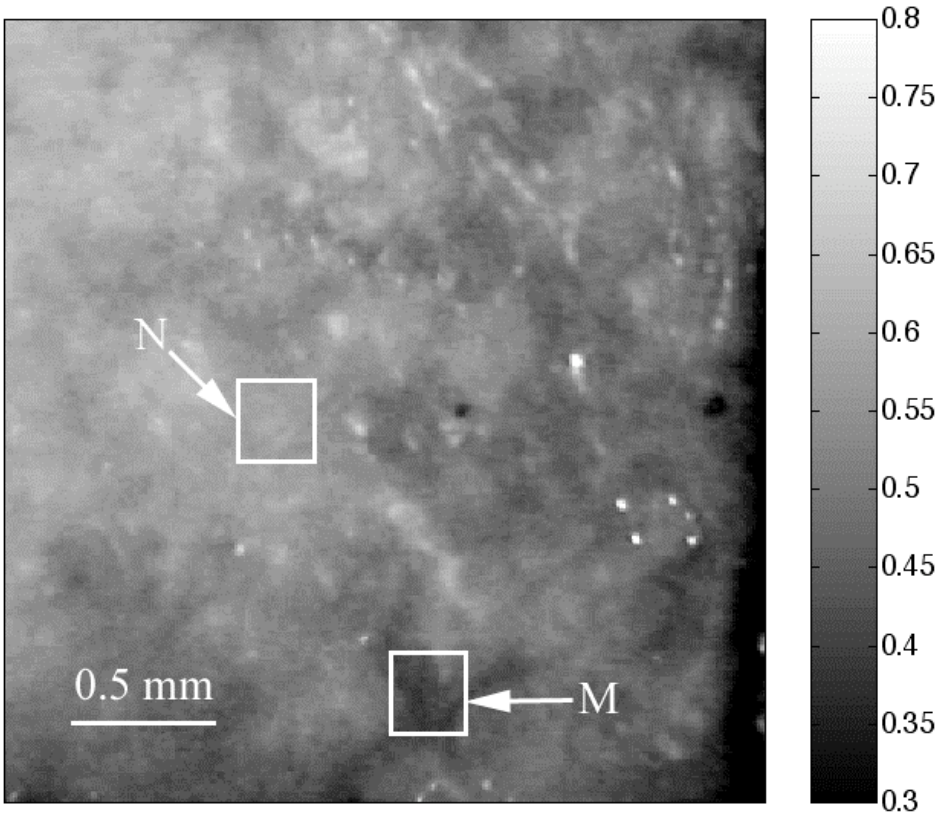

Figure 5a: Normal image of melanoma in situ. Each pixel of the reflectance image was normalized by the average value of a 65% reflectance standard and multiplied by 0.65. White squares denote regions of interest, nonpigmented/amelanotic (N) and melanotic (M), from which data for Fig. 6 is collected.

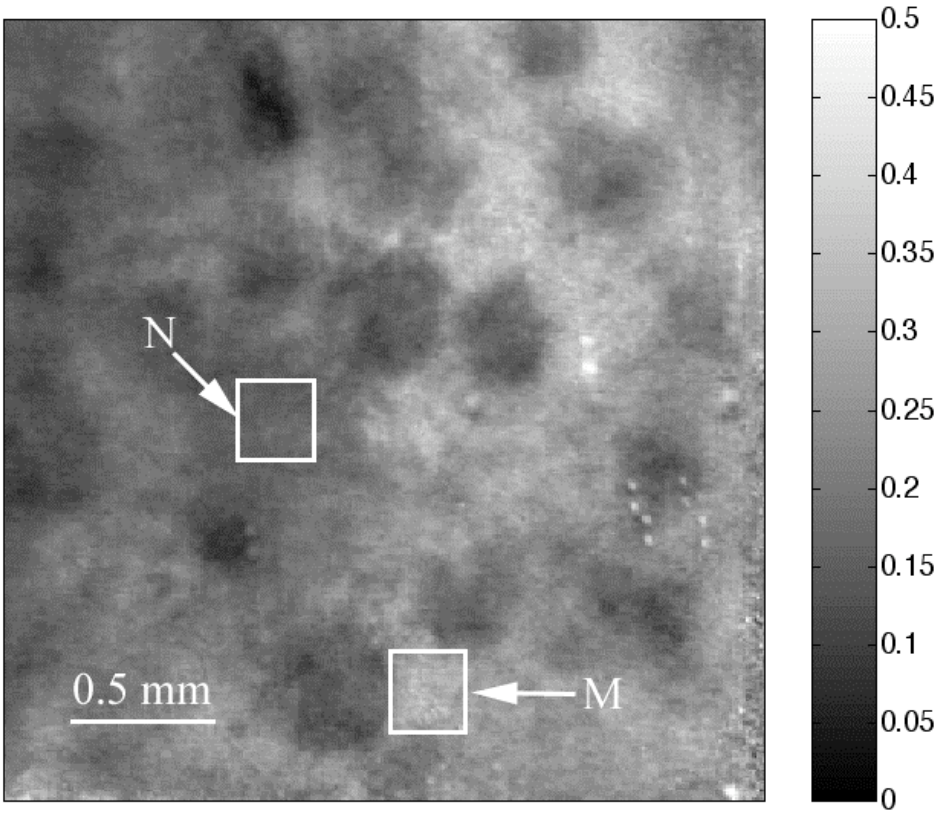

Figure 5b: Polarized image of melanoma. White squares denote regions of interest, nonpigmented/amelanotic (N) and melanoma (M), from which data for Fig. 7 is collected. In this image the grayscale levels are 256.

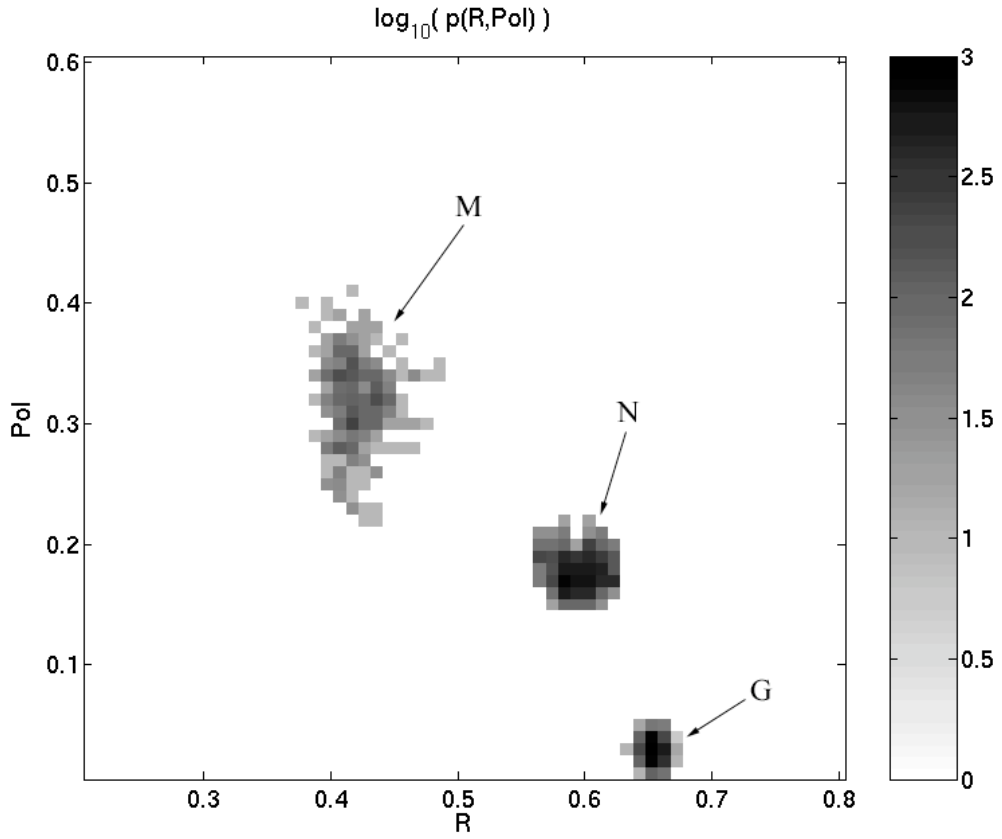

Figure 6: Probability density functions, p(Pol, R), showing the distribution of pixel values versus Pol and R for the visible melanin skin site (M), the non-pigmented normal skin site (N), and the standard gel (G). The p(Pol,R), in units of [R^{-1} Pol^{-1}], is normalized such that the integral of p(Pol,R) for each sample is unity. The greater variation in Pol relative to R for the melanotic site (M) indicates how Pol images present more texture in an image of a variegated melanotic skin lesion.

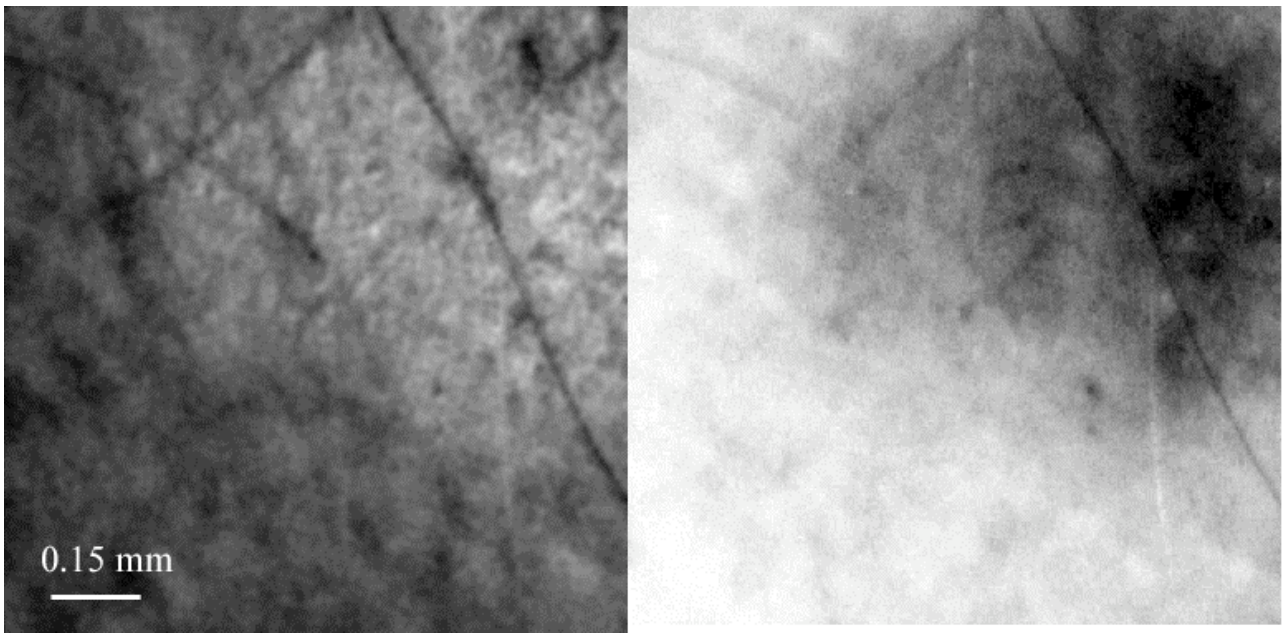

Figure 7: Image of a nevus. The apparent textural structure of the nevus is visible in the polarized image on the left, the grayscale levels of the polarized image were 256. The normal image on the right does not show this structure.

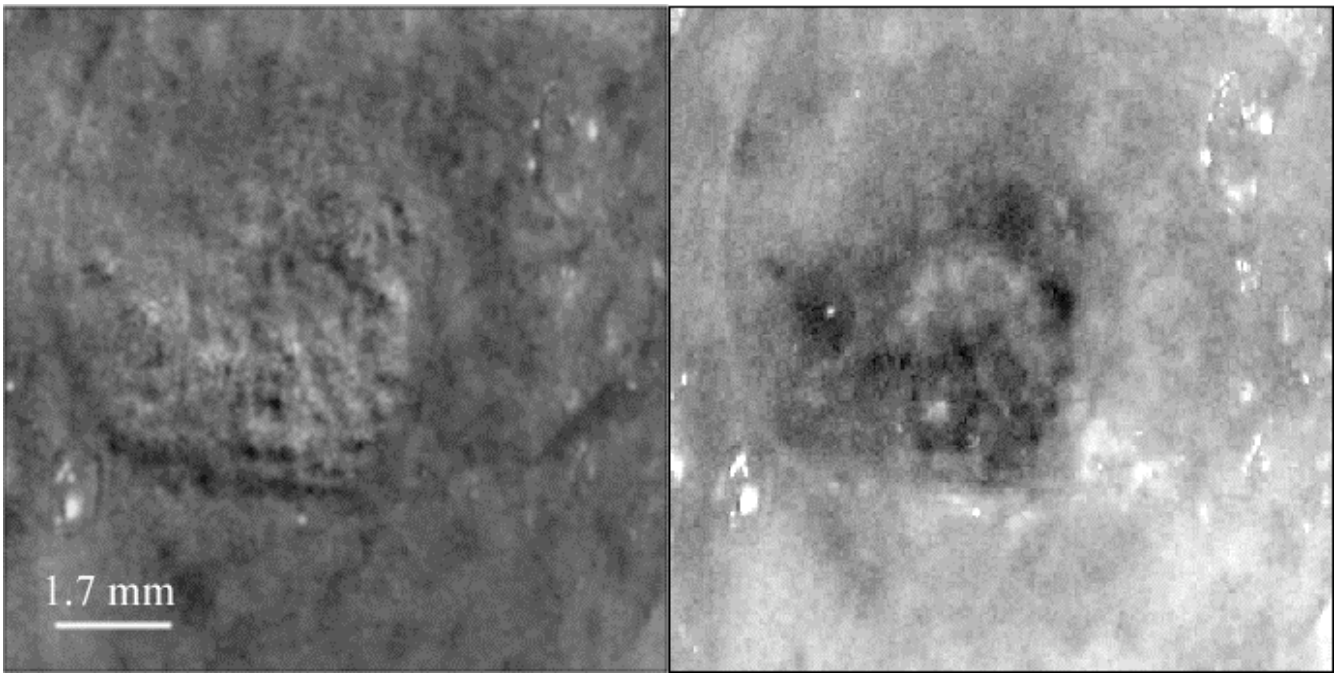

Figure 8: Polarized (left) and normal (right) image of a squamous cell carcinoma on a patient's upper lip. The grayscale levels of the polarized image were 256.

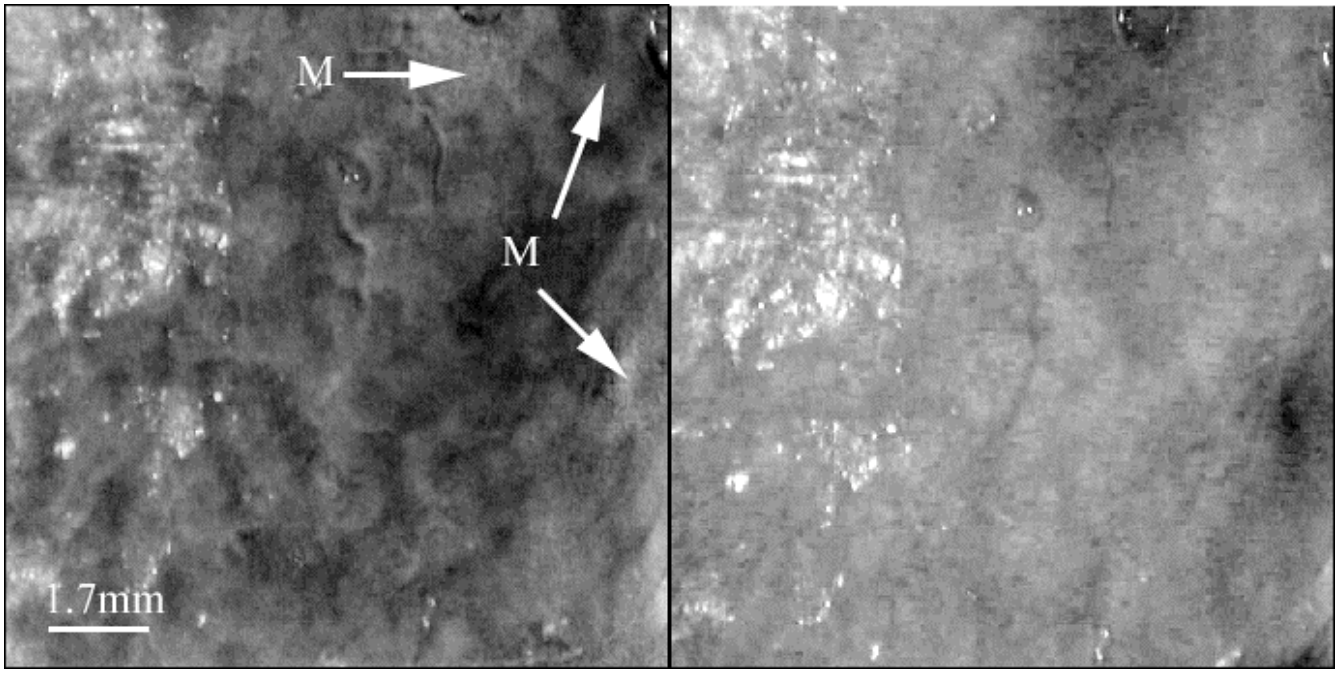

Figure 9: Image of a melanoma on a patient's nose. The melanoma appears dark in the normal image (right) and white in the polarized image. The arrows show branches of the spreading melanoma. This entire area was excised during surgery. The grayscale levels of the polarized image were 256.